RSC Advances

PAPER

View Article Online
View Journal | View Issue

Cite this: *RSC Adv.*, 2017, **7**, 19117

PRAP-CVD: how to design high conformal PEDOT surfaces†

B. R. Pistillo,* K. Menguelti, D. Arl, F. Addiego and D. Lenoble

Received 9th January 2017
Accepted 25th March 2017

DOI: 10.1039/c7ra00343a

rsc.li/rsc-advances

Efficient deposition of polymers on 3D substrates is a key point for many applications where a high surface area is required. Smart textiles based on conductive fibers is one of the most attractive domains where conformal polymer deposition is essential. In this frame, plasma radical assisted polymerization *via* chemical vapour deposition (PRAP-CVD), a solvent-free technique, has been demonstrated to be able to deposit highly uniform poly(3,4-ethylenedioxythiophene) (PEDOT) films. Low temperature of the substrate (<100 °C) and medium vacuum (<50 Pa) combined with good functionality of the films allow the application of PRAP-CVD to a wide range of complex substrates. Polyethylene terephthalate wipers were covered with PEDOT by PRAP-CVD to develop textile-based devices. PRAP-CVD versatility goes beyond the current vapour/solution-based techniques as shown in this work.

Introduction

During the last few decades, the interest in electrically conductive fibres for several applications such as medical, sports, military, and energy has increased significantly.[1,2] The way in which conventional conductive materials can be processed into/onto textiles revealed a tough challenge also because garments should be comfortable rather than hard and rigid when worn. Three types of conductive materials have been mainly explored for the fabrication of conductivity textiles: metallic-based, carbon-based and polymeric materials.[3–5] For example, metal monofilaments, metal fibres or metal wires can be blended with all sorts of fibres or can be directly used in weaving and knitting.[6,7] Carbon-nanotube (CNT) fibres owing to their intriguing properties such as electrical conductivities, mechanical strength and structural flexibility are also promising candidates in wearable electronic textiles. To this end, several methods were developed including wet spinning of fibres from a CNT solution, dry spinning of fibres from either a nanotube forest or chemical vapour deposition.[8,9] The health hazards caused by carbon black or CNT and limited textile applications of metallic fillers along with their high stiffness, high weight, high cost and low compatibility with other constituents pushed scientists toward new solutions. Intrinsically conductive polymers (ICPs) are currently considered as an alternative to conventional conductive materials.[6,10] ICPs also provide all the desirable aspects of polymers, mechanical flexibility, robustness and low cost can be preserved along with good electrical conductivity.[11,12] Among ICPs, for smart textiles production, several attempts have been done by using poly(3,4-ethylenedioxythiophene):poly(styrene sulfonic acid) (PEDOT:PSS) owing to its good electrical and mechanical properties.[13] Nevertheless many drawbacks, mainly attributed to the presence of PSS such as acidity, poor chemical stability *etc.*, limit the application of this solution to some restricted type of surfaces.[14] It is also important to highlight the presence of phenomena like dewetting, low surface adherence and surface tension hindering in the case of PEDOT solutions deposition on micro/nano-textured surfaces.[15,16] To circumvent part of the mentioned shortcomings, ICPs can be deposited through vapour phase polymerization where the solubility of the conjugated monomer is no longer required.[17] Most of vapour phase depositions focus on yarn covering resulting in a poorly connected and not conformal conductive material that exhibits delamination.[18] Where a solution of $FeCl_3$ is used as oxidant, the polymerization process strictly depends on the ability of textile to absorb the oxidant.[19] Furthermore, during the knitting, rubbing phenomena can occur. As a consequence, part of deposition can be removed modifying film thickness and performance.[11]

Plasma radicals assisted polymerization *via* CVD (PRAP-CVD) is emerging as an efficient alternative to conventional vapour-based technique to synthesise and deposit conjugated polymers.[20] The low deposition temperatures, below 100 °C, allow polymers to be directly synthesised on a wide range of substrates, including paper and plastic, without any thermal degradation. Additionally, the PRAP-CVD does not require post-deposition rinsing procedure. In this study we demonstrated the advantage of depositing PRAP-CVD PEDOT directly on the fabric. Polyethylene terephthalate (PET), more commonly referred to as

Department of Materials Research and Technology, Luxembourg Institute of Science and Technology, 5, Avenue des Hauts Fourneaux, L-4326 Esch sur Alzette, Luxembourg. E-mail: tillo@list.lu; Fax: +352 27 58 85; Tel: +352 275.888.586

† Electronic supplementary information (ESI) available. See DOI: 10.1039/c7ra00343a

polyester, was chosen as reference textile since it is one of the most commonly used polymers in textile industry both as fibres and fabrics because of its high strength, low moisture absorption, and resistance to shrinkage which fulfil fibre industry specifications.

We combined the advantage of PRAP-CVD, as substrate-independence process and the conformality of produced film, to obtain efficient conductive PET fabric. PEDOT did not alter functional properties of the textile and withstand substrate drawing. This study highlights the potential of PRAP-CVD as a scalable and commercially feasible method with unique capabilities in terms of conformality.

Results and discussion

Thin PEDOT nanofilms having a very large surface/thickness ratio were deposited on several textiles as reported in Fig. 1. Complex 3D substrates as PET fabrics (Fig. 1a), cotton fabrics (Fig. 1b), linen fabrics (Fig. 1c) and paper cellulose fibres (Fig. 1d) were successfully treated by PRAP-CVD demonstrating the conformality of this technique. The rest of the paper focused on PET fabrics as reference substrate.

The polymerization mechanism of EDOT to form PEDOT is described elsewhere.[21] In essence, the production of bromine plasma radicals began a free-radical polymerization of the EDOT at the substrate surface. The polymerization stopped when last α' position available was brominated. The obtained polymerization was firstly attested by optical microscopy (OM), as reported in Fig. 2. Before the deposition the PET wipe appeared white while just after the process, it changed colour appearing bluish. In the oxidized state, cations generated every five EDOT monomer segments are charge balanced with anions in the vicinity. The electronic arrangement is shown schematically in Fig. 3. The counter ion for PRAP-CVD is bromine. The unpaired electrons are delocalized along the PEDOT backbone, resulting in conductive behaviour of PEDOT. In this highly energetic state, the electrons absorb mostly low-energy near-infrared light and are relatively transparent to visible light. In the reduced state, the electrons are most stable in the conjugated alternating single/double bond configuration. Due to resonance, the electrons are delocalized over a few polymer segments. The conjugated electrons are at a lower energy than unpaired electrons, and absorption is shifted into the higher energy visible region, resulting in the dark colour.[22,23] The conformity of film on the fibres is a key point in the list of industrial requirements. Conductive PEDOT films were deposited on standard PET fabric to demonstrate functional conformal films. Scanning electron microscopy (SEM) investigation was carried out to prove the effectiveness of the technique. A comparison before and after PRAP-CVD process is reported in Fig. 4. Correspondence of the textile morphology between the uncoated and coated sample illustrated the high conformal coverage of the fibres with thin film of polymer (Fig. 4a and b). The presence of PEDOT sustained by the changing in colour and preserved morphology was confirmed by Energy Dispersive X-ray spectroscopy (EDX) in Fig. 4c and d, respectively. In the spectrum of PET, peaks of carbon (C) Kα at 0.3 keV and oxygen (O) at 0.5 keV were detected while the spectrum of fibres treated *via* PRAP-CVD highlighted the presence of sulphur (S) at 2.3 keV and bromine (Br) at 11.9 keV. Sulphur as well as carbon and oxygen were attributed to the chemical composition of EDOT while bromine was present as dopant. PEDOT film resulted in defect/pin-hole free, as attested by the high magnification SEM micrographs. In order to deeply prove this peculiarity of PRAP-CVD, a stripe of PET fabric covered with PEDOT was cut by means a scalpel and analysed by SEM. In Fig. 5, micrographs of the same PEDOT/PET area, recorded at different magnifications, are reported (Fig. 5a and c). The cut induced a physical convergence of fibres. The light area could be attributed to the PEDOT which responded differently from PET to the irradiation of the electron beam. The presence of PEDOT

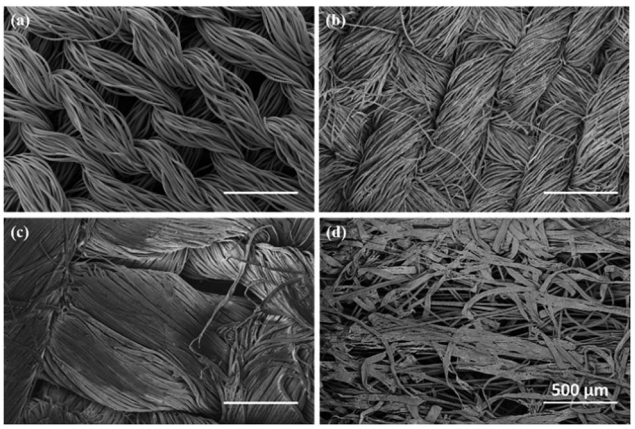

Fig. 1 SEM microscopies of PRAP-CVD PEDOT on (a) PET fabric, (b) cotton fabric, (c) linen fabric and (d) paper cellulose fibres. Samples have been investigated after the deposition without any further manipulation.

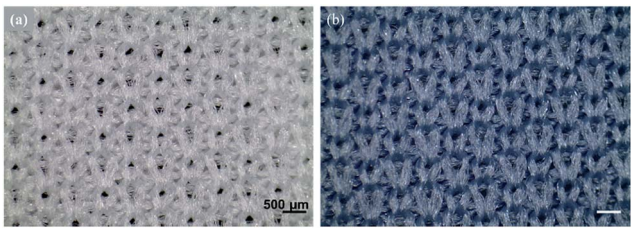

Fig. 2 Optical microscopy images of (a) untreated knitted PET fabric microstructure appearing with a white colour, and (b) knitted PEDOT/PET fabric microstructure appearing with a blue one.

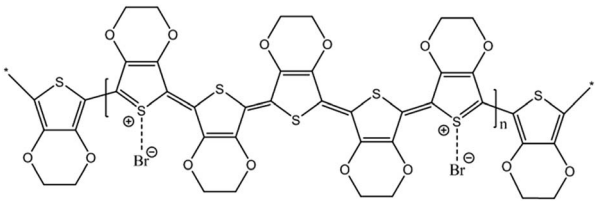

Fig. 3 Electronic arrangement of PEDOT doped with bromine. Oxidised PEDOT showed a light sky blue colour.

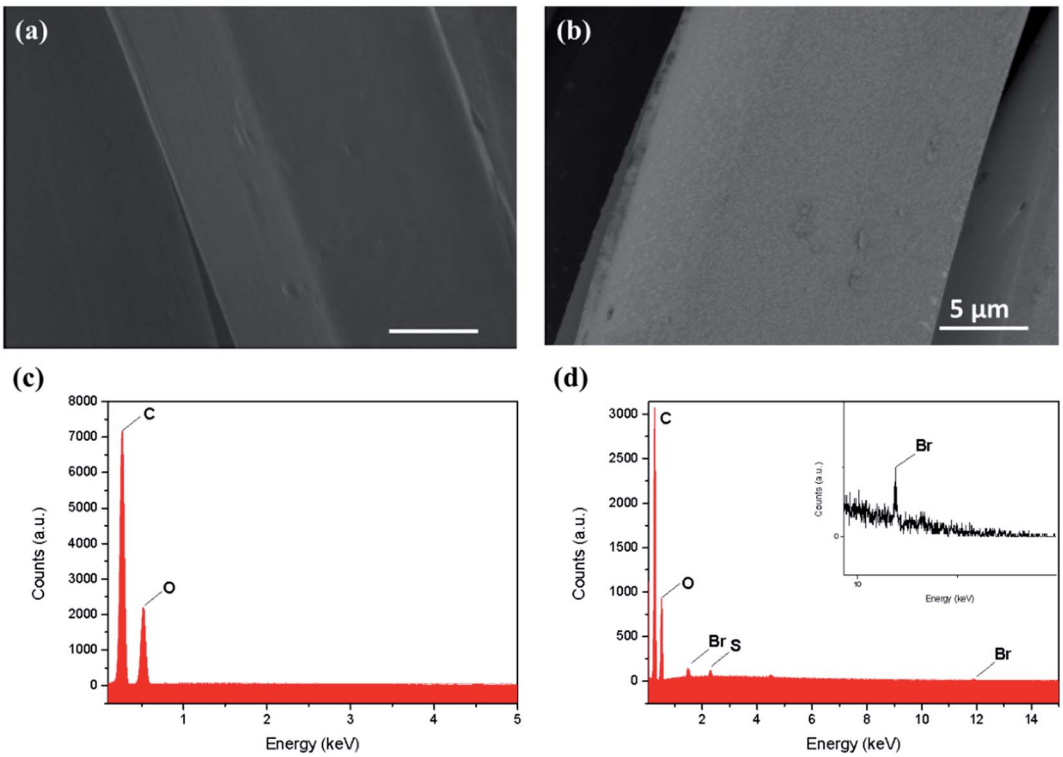

Fig. 4 SEM images of textile fibres (a) before and (b) after the PRAP-CVD process. Owing to the induced conductivity of PEDOT, the two images resulted in different colour, darker the raw PET and lighter the PEDOT/PET fiber. Respective EDX spectra identified the presence of (c) carbon and oxygen in raw PET and (d) also sulphur and bromine residues in the PEDOT coated fabric.

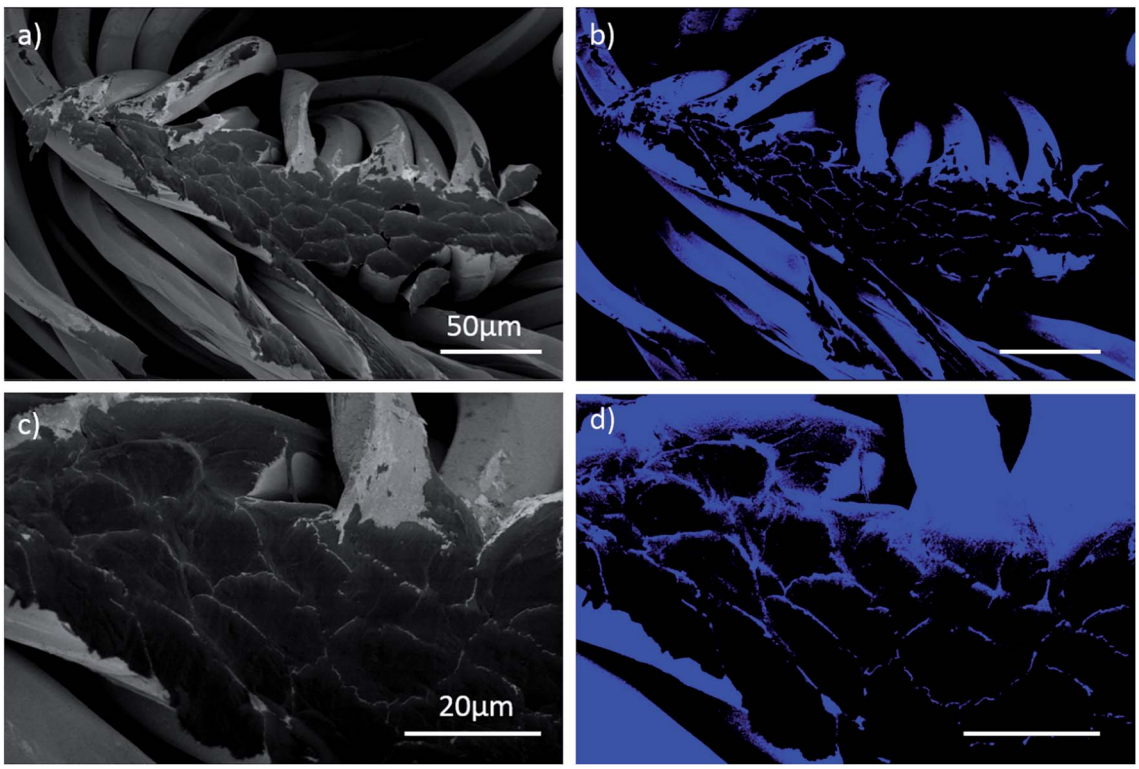

Fig. 5 SEM micrographs of PET fibres cross-section with PEDOT film (a, c) at different magnification; (b, d) corresponded coloured picture at same magnification. The dark area corresponded to PET fibres. Conductive PEDOT film responded differently from PET while irradiated by the electron beam.

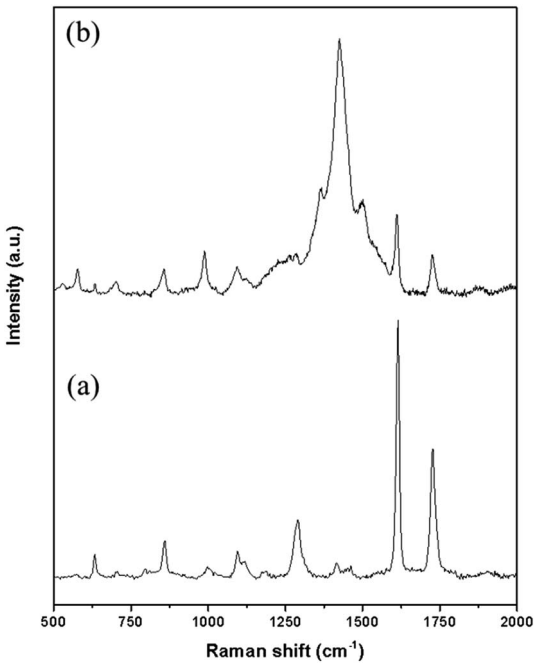

Fig. 6 Raman spectra of (a) untreated PET, (b) PET/PEDOT at an excitation wavelength of 633 nm.

was also confirmed by the rip of fibres owing to movement of scalpel. A video attesting this behaviour is present in ESI† document. The same images were also artificially coloured by Image J software (Fig. 5b and d) to easily identify the layer of PEDOT which conformably surrounded each fibre although the convergence of fibres.

Following FIB cross-sectioning step, an accurate thickness measurement of film deposited all around the textile fibres was determined. A thickness of (215 ± 10) nm allowed to establish a deposition rate of 6 nm min^{-1}. This level of coating quality is unparalleled to current wet and dry PEDOT synthesis.[24,25]

Raman investigation was carried out to prove PEDOT polymerization by determining the vibrational modes of spectra. The Raman spectra of PEDOT/PET and of the untreated PET, measured at excitation wavelengths of 633 nm, are displayed in Fig. 6. In the Raman spectrum of pure PET fabric (Fig. 6a), two strong characteristic bands appeared at 1729 cm^{-1} and 1615 cm^{-1}, which corresponded to the C–O stretching vibration and benzene ring stretching vibration, respectively. Weak band at 1415 cm^{-1} could be attributed to the aromatic ring C–C stretching vibration and $–OCH_2–$ wagging vibration. The bands that identified methylene group, owing to the C–H deformation vibration and the CH_2 wagging vibration, were observed at 1461 cm^{-1} and 1290 cm^{-1}, respectively. The asymmetric C–O–C stretching also contributed to the last band. The band at 1182 cm^{-1} was owing to the symmetric C–O–C stretching. The ester C(O)O bending mode was attributed to the band at 859 cm^{-1} while the band generated by the in-plane deformation vibration of the C(O)O group, characteristic for aromatic esters, was detected at 632 cm^{-1}.[25–27] The spectrum of PEDOT/PET in Fig. 6b showed low-intensity bands at 579 cm^{-1} and 989 cm^{-1}, ascribed to the oxyethylene deformation. The band at 707 cm^{-1} and 1262 cm^{-1} corresponded to symmetric C–S–C deformation and Cα–Cα′ (inter-ring) stretching modes, while that at 1370 cm^{-1} was attributed to the Cβ–Cβ stretching. The symmetric Cα=Cβ (–O) stretching was assigned at 1426 cm^{-1} and the asymmetric Cα=Cβ stretching at 1514 cm^{-1}.[21,28] The other bands could be attributed to the presence of substrate beneath.

It was also possible to determine chemical states of PET and PEDOT/PET C 1s respectively, by X-ray Photoelectron Spectroscopy (XPS), as presented in Fig. 7. The atom in the untreated PET spectrum, Fig. 7a, was present in three chemical states, reflecting the presence of the three peaks: C1 at binding energy of 284.5 eV that corresponded to C–C/H bond (aliphatic/aromatic carbon atoms), C2 at 286.0 eV attributed to C–O bond (methylene carbon atoms singly bonded to oxygen), and C3 at 288.5 eV recognised as signal owing to –COO– bond (ester carbon atoms). Last, the broad small peak at 291 eV corresponded to the π–π* shake-up transition associated with the aromatic ring of the PET.[29] The best fitting procedure allowed attributing the following percentage areas: 54.2% C1, 24.6% C2, 14.6% C3, and 6.6% shake-up. In Fig. 7b, the distribution of functional groups of PEDOT C 1s showed three different components: C1 represented C–C/H bonds, depicted at 284.4 eV, C2 attributed to C–S at 285.5 eV and C–O at 286.1 eV. An asymmetrical peak at about 288 eV owing to the contribution from the π → π* shake-up transition and positively polarized or charged carbon was also identified. Peak areas were calculated as 34.8% for C–C/H, 42.5% for C–S, 17.3% for C–O and 5.4% for the shake-up.[30] Best-fitting procedure was also applied to core-level of O 1s and S 2p. In particular, S 2p core-level

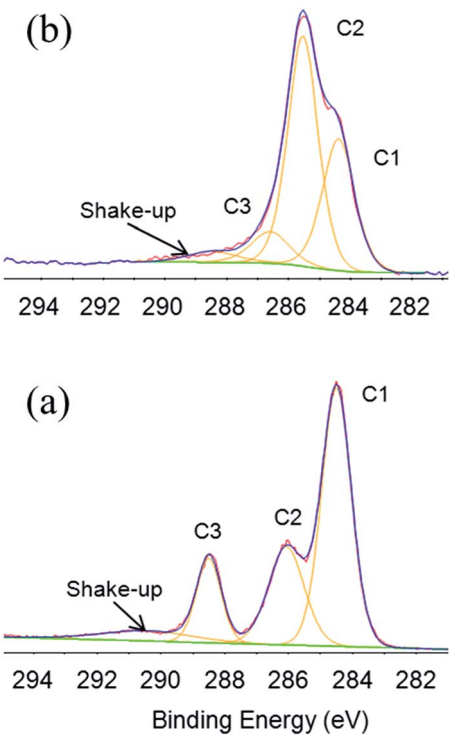

Fig. 7 XPS C 1s high resolution spectra of (a) PET and (b) PEDOT/PET and relatively chemical states.

spectrum corresponded to single sulphur bonding environment in PEDOT with a spin-split doublet, $2p_{1/2}$ and $2p_{3/2}$ separated by 1.18 eV in binding energy and an area ratio 1 : 2, as presented elsewhere.[21] The presence of the asymmetric tail at higher binding energy was related to the doping process, in which the delocalized π-electrons in thiophene ring broaden the binding energy spectrum of the sulphur atom.[31] The quantitative analysis of PEDOT film showed the followed atomic percentage of 66% C, 21% O, 9% S, and 4% Br.

The resistance of PEDOT coating to drawing was investigated by *in situ* tensile testing of PET fabric in an environmental pressure SEM at a temperature of 20 °C and at a strain rate of 0.0025 s^{-1}. The typical stress–strain curve of PEDOT/PET subjected to tensile testing is shown in Fig. 8. A comparison between the raw and covered fabrics was reported. In the case of PEDOT, three steps were identified: (i) from 0% to about 9% of strain, a marked increase of stress was observed certainly due to the intrinsic stiffness of the fabric, (ii) from 9% to 80% of strain, a stabilisation of stress was noted probably owing to the progressive rearrangement of the fabric fibres around the knits, and finally (iii) above 80% of strain, a high increasing of the stress was observed reflecting one more time a high tensile strength. This last stage of strain-hardening could suggest the drawing of the fibres oriented in the tensile direction and the drawing of the knits exhibiting resistance to the imposed strain. Note that the tensile behaviour of the different fabrics was only representative up to 90% of strain, and then the tensile behaviour was not repeatable due to activation of different mechanisms of edge fabric damage and fabric rupture yielding to different intensities of strain-hardening. A quite similar tensile behaviour could be identified in the case of raw fibres, attesting the low influence of PEDOT on the fabric mechanical properties.

SEM investigation was performed to check possible damage of fibres during and after the traction. As reported in Fig. 9a, SEM micrographs of fabric at its maximum strain of 175% was recorded and compared with that of the fabric after unloading corresponding to a strain of 100%, Fig. 9b. The film did not show any evidence of damage or morphology change indicating

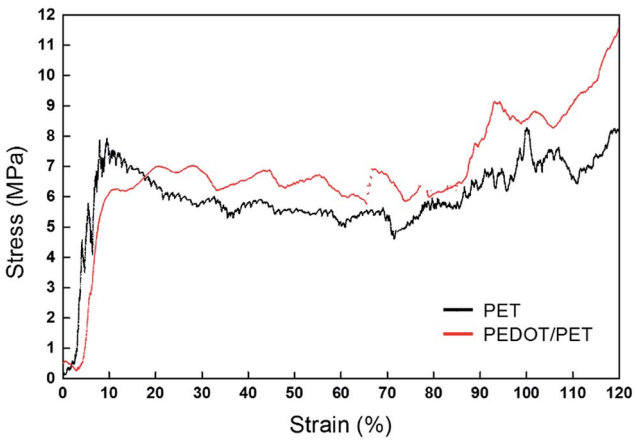

Fig. 8 Typical stress *vs.* strain curves of untreated PET fabric and PEDOT/PET fabric at 0.0025 s^{-1} and 20 °C.

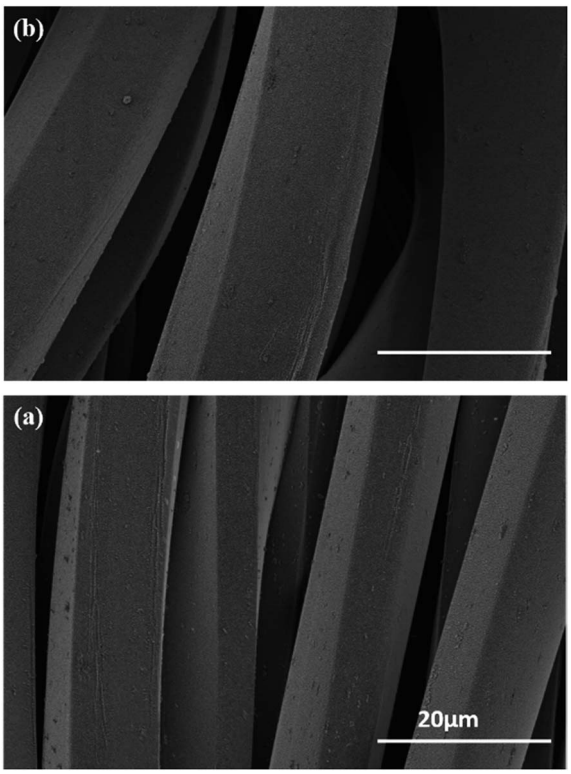

Fig. 9 SEM images of PEDOT/PET at (a) strain of 175% before unloading and (b) relaxed state after unloading corresponding to a strain of 100%.

that the film withstand drawing with a high elasticity. Even in the extreme case of locally broken PET fibres, PEDOT adhered strongly to the PET, since no crack was detected on the part which remained on the substrate.

This finding demonstrated that PRAP-CVD allowed a high conformal deposition bypassing the poor connectivity and the delamination phenomena common to the other techniques.[24] For all experiments run any modification in the morphology of samples was detected during the unloading stage. This result could support the hypothesis that PEDOT can also withstand the relaxation of PET fabric, probably due to a high intrinsic elasticity.

Fabric properties, in terms of conductivity, were modified with the presence of PEDOT, as anticipated by SEM analyses. Any resistance could be measured on the raw PET substrate, while when it was processed an electrical resistance of 35.19 MΩ was found. Similar values in terms of sheet resistance were measured also after drawing, attesting the high degree of elasticity of film chains. Considering the thickness of film measured *via* cross-section SEM, the conductivity of film was estimated to be 3 S cm^{-1}, which is a promising value considering the uncountable advantages of PRAP-CVD compared to the other CVD techniques.

Finally, the size of sample is also a parameter which diversify PRAP-CVD to the current CVDs, samples up (15 cm × 15 cm) can be treated. In the Fig. 10, an example of PEDOT/PET (13 cm × 13 cm) has been reported.

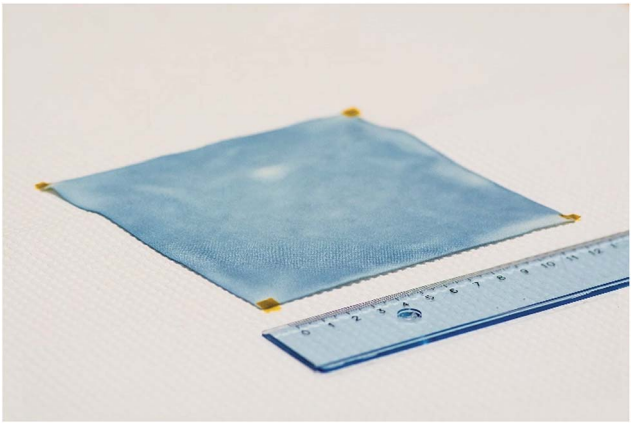

Fig. 10 Picture of (13 cm × 13 cm) PET fabric covered by PRAP-CVD PEDOT film.

A large area of sample could covered with PEDOT revealing a quite good degree of uniformity. The homogeneous temperature all over the substrate is a key aspect of PRAP-CVD and it is obtained by a good balance between the vacuum and the adhesion of the sample to the sample holder.

In order to facilitate the readability of paper an ESI† wad added.

Experimental

Materials

PRAP-CVD of PEDOT films was carried out on laundered knitted polyester wipers (20 cm × 20 cm), (VWR, USA) without any treatment.

3,4-Ethylenedioxythiophene (EDOT, 97%) and bromine (puriss. p.a., ≥99.0%), Sigma-Aldrich (Belgium), were used as received to deposit PEDOT film. The deposition took place in the PRODOS-200 PVPD™ R&D System-β version (AIXTRON SE, Herzogenrath, Germany).

EDOT monomer vapour was delivered into the reactor by a TriJet® ($\varphi_{EDOT} = 4.2 \times 10^{-3}$ mol min^{-1}) and bromine by a bubbler system ($\varphi_{Br2} = 6.8 \times 10^{-4}$ mol min^{-1}). The different pathways allowed a well separated injection of monomer and oxidant. Any mix occurred whilst mingling the respective jet in the reactor close to the surface of the substrate. The substrate temperature was set to 80 °C while the reactor pressure was kept constant at 390 mTorr by a throttle valve.

Film characterization

Raman spectroscopy. The Raman spectra were recorded by a Renishaw inVia micro-Raman spectrometer, with an incident wavelength of 633 nm and a laser power below 10 mW.

X-ray photoelectron spectroscopy. XPS analyses were carried out with an Axis Ultra DLD Spectrometer (Kratos Analytical Ltd., UK; Al Kα $h\nu = 1486.6$ eV, 400 μm × 700 μm spot). Spectra were analysed by Thermo Scientific™ Avantage Data System.

A dual-beam focused ion beam (FIB) and scanning electron microscopy (SEM). Helios NanoLab™ 650 (FEI, Eindhoven, Netherland) was used to investigate the morphology of deposited film with an acceleration voltage of 2 kV, a current of 25 pA, and a working distance of 4 mm. No electron surface charging occurred, and hence, no metal coating was needed. FIB cross-sections were prepared by depositing a Pt protection layer followed by the sectioning using a Ga-ion beam working at 30 kV and currents between 7 pA and 80 pA. Major precautions were taken to minimize the impact of the ion-beam on the material.

Microscopic *in situ* tensile testing. A miniature tensile/compression module Kammrath & Weiss coupled with SEM was used for carring out a stretch test *in situ*. This machine was equipped with a 5 kN load cell providing a 1 N resolution within all the load range, while the sample displacement was recorded by means of a linear variable differential transformer (LVDT) parallel to the lead screws. Testing was done at SEM chamber temperature room temperature (about 20 °C). Rectangular samples with an initial length of about 20 mm and initial width of about 5 mm were tested with an initial gauge length L_O of about 8 mm at a crosshead displacement speed $\Delta L/\Delta t$ of 20 μm s^{-1}. The strain ε (in %) was calculated as $100 \times (\Delta L/L_O)$ and the corresponding strain rate $\Delta\varepsilon/\Delta t = 1/L_O \times \Delta L/\Delta t$ was evaluated to be 0.0025 s^{-1}. Note that the samples were carefully cut by means of a razor blade with their long axis (lengths) always oriented in the same fabrics direction. Once the strain levels of interest were reached during the tensile stage, it was kept constant and SEM measurements were conducted during several minutes. Therefore, some inherent load relaxation of the sample occurred. During this testing, a second SEM model Quanta FEG 200 from FEI (Eindhoven, The Netherlands) was utilized and was specifically designed to hold the miniature tensile/compression module. The images were recorded at a water pressure of 150 Pa with the Large-field detector (LFD) enabling to record secondary electron images.

Electrical properties. Film electrical resistance was measured using a 2-points probe Fluke 179 True RMS Digital Multimeter.

Optical microscopy. The microstructure of the textiles was revealed by a stereo microscope model SZ61 from Olympus.

Conclusions

By using PRAP-CVD, PEDOT films were successfully deposited on complex 3D substrates as PET fabrics, cotton fabrics, linen fabrics and paper cellulose fibres. The use of different substrates demonstrated the versatility of this technique in terms of applications. PET fabrics was chosen as reference substrate to demonstrate the conformality of PRAP-CVD.

Surface physical–chemical characterizations as XPS, EDX and Raman spectroscopy highlighted the homogeneous covering of PEDOT all around the fabrics and its independence from the kind of substrate. The behaviour of PEDOT when undergone to mechanical stress, revealed that the film withstand drawing with a high elasticity. By this technique is therefore possible modify only the surface of substrate without interfering with its bulk properties.

The conformal nature of PRAP-CVD PEDOT, highlighted by SEM micrographs, make an easy possibility the modification of objects having complex shapes.

In conclusion, PRAP-CVD polymerization produced conformal coatings, which precisely followed the geometry of the underlying substrate independently from its nature. The mild experimental conditions permitted its application to a wide range of substrates. The deposition, developed in a pre-industrial machine, can be carried out on 8-inch silicon wafer as well as 15 cm × 15 cm squared samples.

To our best knowledge, this is the most conformal way to deposit polymeric film all around textiles. This work also highlighted the industrial maturity of this novel technique and the easy scaling up of this process featuring highly competitive growth rate compared to other vapour phase growth of PEDOT thin-films.

Acknowledgements

The authors wish to express their appreciation to Dr Mael Guennou, Dr Jerome Guillot and Dr Yves Fleming for the performed Raman and XPS analyses, respectively, and to Mr Jean-Luc Biagi for conducting SEM imaging during *in situ* tensile testing. Dr Renaud Leturcq is also thanked for fruitful discussions. A further acknowledgment is owing to Mme Lugdivine Unfer for the picture reported in Fig. 10. This work has been funded in part by Fond National de la Recherche Luxembourg (FNR Luxembourg) through INTER/NSF/MAT/11/01 "Visible Light Nanocomposite Photocatalysts" (VISICAT) project.

References

1 V. Koncar, *NoSmart Textile and Their Applictions*, Woodhead Publishing, 1st edn, 2016.
2 L. W. Adams, M. W. Gilpatrick, and R. V. Gregory, Fabric having non-uniform electrical conductivity, *US Pat.* 5316830, 1992.
3 B. K. Little, Y. Li, V. Cammarata, R. Broughton and G. Mills, *ACS Appl. Mater. Interfaces*, 2011, **3**, 1965–1973.
4 B. S. Shim, W. Chen, C. Doty, C. Xu and N. A. Kotov, *Nano Lett.*, 2008, **8**, 4151–4157.
5 Y. Ding, M. A. Invernale and G. A. Sotzing, *ACS Appl. Mater. Interfaces*, 2010, **2**, 1588–1593.
6 D. Meoli and T. May-plumlee, *Journal of Textile and Apparel, Technology and Management*, 2002, **2**, 1–12.
7 C. Lawrence, *High Performance Textile and Their Applications*, Woodhead Publishing, Sawston, Cambridge (UK), 2014.
8 Y. Shang, X. He, Y. Li, L. Zhang, Z. Li, C. Ji, E. Shi, P. Li, K. Zhu, Q. Peng, C. Wang, X. Zhang, R. Wang, J. Wei, K. Wang, H. Zhu, D. Wu and A. Cao, *Adv. Mater.*, 2012, **24**, 2896–2900.
9 Y. Inoue, K. Kakihata, Y. Hirono, T. Horie, A. Ishida, H. Mimura, Y. Inoue, K. Kakihata, Y. Hirono, T. Horie and A. Ishida, *Appl. Phys. Lett.*, 2012, **213113**, 10–13.
10 T. Bashir, J. Naeem, M. Skrifvars and N. Persson, *Polym. Adv. Technol.*, 2014, **25**, 15018–21508.
11 M. Stoppa and A. Chiolerio, *Sensors*, 2014, **14**, 11957–11992.
12 P. Kovacik, G. Hierro, W. Livernois and K. K. Gleason, *Mater. Horiz.*, 2015, **2**, 221–227.
13 H. Okuzaki, Y. Harashina and H. Yan, *Eur. Polym. J.*, 2009, **45**, 256–261.
14 L. Wengeler, K. Peters, M. Schmitt, T. Wenz, P. Scharfer and W. Schabel, *J. Coat. Technol. Res.*, 2014, **11**, 65–73.
15 F. Zhang, M. Johansson, M. R. Andersson, J. C. Hummelen and O. Inganäs, *Adv. Mater.*, 2002, **14**, 662–665.
16 Y.-K. Han, M.-Y. Chang, W.-Y. Huang, H.-Y. Pan, K.-S. Ho, T.-H. Hsieh and S.-Y. Pan, *J. Electrochem. Soc.*, 2011, **158**, K88–K98.
17 B. Winther-Jensen and K. West, *Macromolecules*, 2004, **37**, 4538–4543.
18 T. Bashir, M. Skrifvars and N. Persson, *Polym. Adv. Technol.*, 2011, **22**, 2214–2221.
19 T. Bashir, M. Skrifvars and N. Persson, *Polym. Adv. Technol.*, 2012, **23**, 611–617.
20 B. R. Pistillo, K. Menguelti, C. Bizzarri, M. Kunat, J. Kreis, M. Heuken and D. Lenoble, in *13th Flexible & Printed Electronics Conference & Exhibition*, Phoenix, 2014.
21 B. R. Pistillo, K. Menguelti, N. Desbenoit, D. Arl, R. Leturcq, O. M. Ishchenko, M. Kunat, P. K. Baumann and D. Lenoble, *J. Mater. Chem. C*, 2016, **4**, 5617–5625.
22 F. Jonas, B. Ag and Z. B. Zentrale, *Synth. Met.*, 1991, **43**, 831–836.
23 J. Kawahara, P. A. Ersman, I. Engquist and M. Berggren, *Org. Electron.*, 2012, **13**, 469–474.
24 A. K. Sen, *Coated textile*, Taylor & Francis Group, 2nd edn, 2008.
25 V. Kaushik, J. Lee, J. Hong, S. Lee, S. Lee, J. Seo, C. Mahata and T. Lee, *Nanomaterials*, 2015, **5**, 1493–1531.
26 M. B. Radoičić, M. V. Milošević, D. S. Miličević, E. H. Suljovrujić, G. N. Ćirić-Marjanović, M. M. Radetić and Z. V. Šaponjić, *Surf. Coat. Technol.*, 2015, **278**, 38–47.
27 E. Rebollar, S. Pérez, M. Hernández, C. Domingo, M. Martín, T. A. Ezquerra, J. P. García-Ruiz and M. Castillejo, *Phys. Chem. Chem. Phys.*, 2014, **16**, 17551–17559.
28 S. Garreau, G. Louarn, J. P. Buisson, G. Froyer and S. Lefrant, *Macromolecules*, 1999, **32**, 6807–6812.
29 G. Beamson and D. Briggs, *High Resolution XPS of Organic Polymers*, The Scienta ESCA 300 database John Wiley & Sons, 1992, vol. 15.
30 D. Bhattacharyya and K. K. Gleason, *Chem. Mater.*, 2011, **23**, 2600–2605.
31 C. J. Mathai, S. Saravanan, M. R. Anantharaman, S. Venkitachalam and S. Jayalekshmi, *J. Phys. D: Appl. Phys.*, 2002, **35**, 2206–2210.